Anal. Chem. **2007,** *79,* 4977−4986

Model of Vapor-Induced Resistivity Changes in Gold−Thiolate Monolayer-Protected Nanoparticle Sensor Films

William H. Steinecker,[†,‡] Michael P. Rowe,[†] and Edward T. Zellers*[†,§]

Engineering Research Center for Wireless Integrated MicroSystems, Departments of Chemistry and Environmental Health Sciences, University of Michigan, 109 South Observatory, Ann Arbor, Michigan 48109-2029

An investigation of the modulation of charge transport through thin films of *n*-octanethiolate monolayer-protected gold nanoparticles (MPN) induced by the sorption of organic vapors is presented. A model is derived that allows predictions of MPN-coated chemiresistor (CR) responses from vapor−film partition coefficients, and analyte densities and dielectric constants. Calibrations with vapors of 28 compounds collected from an array of CRs and a parallel thickness-shear-mode resonator are used to verify assumptions inherent in the model and to assess its performance. Results afford insights into the nature of the vapor−MPN interactions, including systematic variations in apparent film swelling efficiencies, and show that the model can predict CR responses typically to within 24%. Using CRs of different dimensions, vapor sensitivities are found to be virtually independent of the MPN film volume over a range of 10^4 (device-area × MPN layer thickness). Sensitivities vary inversely with analyte vapor pressure similarly for the two sensor types, but the CR sensor affords significantly greater signal-to-noise ratios, yielding calculated detection limits in the low-part-per-billion concentration range for several of the analytes tested. The implications of these results for implementing MPN-coated CR arrays as detectors in microanalytical systems are considered.

Facilitated by the versatile synthesis of gold−thiolate monolayer-protected nanoparticles (MPNs) published by Brust et al.,[1] numerous reports have appeared on the characterization of MPNs with various thiolate functionalities and their exploitation in applications ranging from catalysis to biomedical diagnostics.[2−5] One such application employs thin MPN films as interface layers on microfabricated transducers for sensing organic vapors. First reported by Wohltjen and Snow in 1998[6] and since explored by numerous researchers,[7−25] vapor sorption into MPN films causes a reversible change in film resistance that can be detected using underlying interdigital electrodes. These chemiresistors (CRs) can be assembled into arrays wherein each sensor is coated with a different MPN,[13−15] and the response patterns generated can facilitate recognition of vapors in a manner similar to that reported for CRs coated with carbon-loaded insulating polymers (CLIP)[26−28] and polymer-coated sensors employing various transducers.[29−35]

Through multiple reports characterizing the dependence of alkanethiolate MPN film resistances on ligand length and gold core size, it has been established that electronic conduction within such films occurs by electric field-induced tunneling,

* Corresponding author. E-mail: ezellers@umich.edu.
† Department of Chemistry.
‡ Current address: Schlumberger-Doll Research, 1 Hampshire St., MD B453, Cambridge, MA 02139.
§ Department of Environmental Health Sciences.

(1) Brust, M.; Walker, M.; Bethell, D.; Schiffrin, D. J.; Whyman, R. *J. Chem. Soc., Chem. Commun.* **1994**, *7*, 801−802.
(2) Pasquato, L.; Pengo, P.; Scrimin, P. *J. Mater. Chem.* **2004**, *14* (24), 3481−3487.
(3) Daniel, M.-C.; Astruc, D. *Chem. Rev.* **2004**, *104* (1), 293−346.
(4) Templeton, A. C.; Wuelfing, W. P.; Murray, R. W. *Acc. Chem. Res.* **2000**, *33* (1), 27−36.
(5) Rosi, N. L.; Mirkin, C. A. *Chem. Rev.* **2005**, *105*, 1547−1562.
(6) Wohltjen, H.; Snow, A. W. *Anal. Chem.* **1998**, *70* (14), 2856−2859.
(7) Wohltjen, H.; Snow, A. W. PCT Int. Appl. WO A1 9927357, 1999.
(8) Jarvis, N. L.; Wohltjen, H.; Snow, A. W. *Proceedings of the 3rd International Aviation Security Technology Symposium*, Atlantic City, NJ, 2001; pp 639−647.
(9) Snow, A. W.; Wohltjen, H.; Jarvis, N. L. *NRL Review*; Naval Research Laboratories: Washington, DC, 2002.
(10) Foos, E. E.; Snow, A. W.; Twigg, M.; Ancona, M. G. *Chem. Mater.* **2002**, *14*, 2401−2408.
(11) Evans, S. D.; Johnson, S. R.; Cheng, Y. L.; Shen, T. *J. Mater. Chem.* **2000**, *10* (1), 183−188.
(12) Han, L.; Daniel, D. R.; Maye, M. M.; Zhong, C. J. *Anal. Chem.* **2001**, *73* (18), 4441−4449.
(13) Han, L.; Shi, X.; Wu, W.; Kirk, F. L.; Luo, J.; Wang, L.; Mott, D.; Cousineau, L.; Lim, S. I.-I.; Lu, S.; Zhong, C.-J. *Sens. Actuators, B* **2005**, *B106* (1), 431−441.
(14) Cai, Q.-Y.; Zellers, E. T. *Anal. Chem.* **2002**, *74* (14), 3533−3539.
(15) Steinecker, W. H.; Rowe, M.; Matzger, A.; Zellers, E. T. *Proceedings of the 12th International Conference on Solid-State Sensors, Actuators and Microsystems, Transducers '03*, Boston, MA, June 8−12, 2003; p 1343.
(16) Krasteva, N.; Besnard, I.; Guse, B.; Bauer, R. E.; Muellen, K.; Yasuda, A.; Vossmeyer, T. *Nano Lett.* **2002**, *2* (5), 551−555.
(17) Joseph, Y.; Besnard, I.; Rosenberger, M.; Guse, B.; Nothofer, H.-G.; Wessels, J. M.; Wild, U.; Knop-Gericke, A.; Su, D.; Schloegl, R.; Yasuda, A.; Vossmeyer, T. *J. Phys. Chem. B* **2003**, *107* (30), 7406−7413.
(18) Joseph, Y.; Krasteva, N.; Besnard, I.; Guse, B.; Rosenberger, M.; Wild, U.; Knop-Gericke, A.; Schloegl, R.; Krustev, R.; Yasuda, A.; Vossmeyer, T. *Faraday Discuss.* **2004**, *125*, 77−97.
(19) Wessels, J. M.; Nothofer, H.-G.; Ford, W. E.; von Wrochem, F.; Scholz, F.; Vossmeyer, T.; Schroedter, A.; Weller, H.; Yasuda, A. *J. Am. Chem. Soc.* **2004**, *126* (10), 3349−3356.
(20) Yang, C.-Y.; Li, C.-L.; Lu, C.-J. *Anal. Chim. Acta* **2006**, *565* (1), 17−26.
(21) Pang, P.; Guo, Z.; Cai, Q. *Talanta* **2005**, *65* (5), 1343−1348.
(22) Pang, P.; Guo, J.; Wu, S.; Cai, Q. *Sens. Actuators, B* **2006**, *B114* (2), 799−803.
(23) Leopold, M. C.; Donkers, R. L.; Georganopoulou, D.; Fisher, M.; Zamborini, F. P.; Murray, R. W. *Faraday Discuss.* **2004**, *125*, 63−76.
(24) Zamborini, F. P.; Leopold, M. C.; Hicks, J. F.; Kulesza, P. J.; Malik, M. A.; Murray, R. W. *J. Am. Chem. Soc.* **2002**, *124* (30), 8958−8964.
(25) (a) Grate, J. W.; Nelson, D. A.; Skaggs, R. *Anal. Chem.* **2003**, *75* (8), 1868−1879. (b) Grate, J. W. *Anal. Chem.* **2003**, *75*, 6759.

10.1021/ac070068y CCC: $37.00
Published on Web 05/25/2007

whereby adjacent gold cores become charged/discharged as electrons pass through the intercore dielectric medium.[7−10,20,39−41] The relevance of insulated-granular-metal theory[42−45] to MPN film conduction was recognized in several early studies.[36,40−41] In the context of this theory, Terrill et al. proposed the following expression for the bulk resistivity, ρ, of an MPN film:[36]

$$\rho = \tau_o e^{\delta\beta} e^{E_a/kT} \quad (1)$$

where τ_o is a constant pre-exponential tunneling factor, δ is the surface-to-surface intercore spacing, β is the electron tunneling constant, E_a is the tunneling activation energy associated with charging adjacent metal cores (see below), k is Boltzmann's constant, T is the absolute temperature, and it is assumed that the metal cores can be modeled as spheres.

Vapor sorption into the thiolate monolayers swells the MPN film, increasing the distance between gold cores and thereby reducing the rate of electron tunneling. Evans et al. showed that relative resistance changes of MPN-coated CRs are generally proportional to the extent of vapor-induced film swelling.[11] However, changes in the dielectric constant of the intercore matrix should also affect film resistance by changing the activation energy associated with charging adjacent gold cores.[45] Indeed, this factor has been invoked to account for observations that sorption of certain vapors causes a decrease or a negligible change in the resistance of MPN-coated CR sensors, but only in qualitative terms.[6−13,20−22] Although the relevance of eq 1 to MPN-coated CR vapor sensor responses is widely recognized,[6−25] a model describing the relationship between measured changes in resistance and the vapor headspace concentration or the extent of vapor−MPN partitioning has yet to be reported.

We have been exploring the use of MPN-coated CR arrays as detectors in a microfabricated gas chromatograph (μGC).[46−48] For such an application, it is important to miniaturize the CR array and to relate individual CR responses to the physicochemical properties of the analyte vapors and MPNs so that the array can be designed to yield response patterns that convey the greatest amount of information possible about the eluting vapors. With these goals in mind, we performed the study described here using *n*-octanethiolate MPNs as archetypical interfacial thin films on CRs of different sizes and on thickness-shear-mode resonators (TSMRs) operated in parallel, each exposed to as many as 28 different organic vapors. A model is derived from eq 1 that relates the responses from CR sensors explicitly to the air concentration of the vapor, the vapor−film partition coefficient, and the relevant properties of the vapor and MPNs. Some interesting and, heretofore unrecognized, features of MPN-CR sensor responses are revealed. The implications of these results for designing sensor arrays for microanalytical systems are emphasized.

Response Model. Equation 1 portrays the tunneling-based resistivity in MPN films as a function of the intercore spacing and the charging activation energy. The first term represents the probability of an electron tunneling from one core to the next in terms of the near-edge separation distance, δ. The sensitivity of the tunneling rate to the gold core separation is reflected in β.[36] The second term of eq 1 represents the probability of overcoming the energy barrier associated with charging adjacent metal cores. The activation energy for this charging is given by[45]

$$E_a = \frac{e^2}{8\pi} \frac{1}{\epsilon_o \epsilon_{th}} \frac{1}{r_c} \left(1 - \frac{r_c}{r_c + \delta}\right) \quad (2)$$

where e is the charge of an electron, ϵ_o is the permittivity of vacuum, ϵ_{th} is the dielectric constant of the thiolate ligand layer, and r_c is the radius of each metal core.

For a given MPN ligand, vapor uptake into the MPN film will affect the first term in eq 1, to a first approximation, only by a swelling-induced separation of gold cores. This is expected to cause an increase in resistance regardless of the vapor, as is most commonly observed.[6−25] Although β depends on the composition of the intercore matrix, for the low sorbed-vapor concentrations considered in this study, changes in β due to vapor uptake are assumed to be negligible. The second term in eq 1 depends mainly on the dielectric constant of the intercore matrix, which can change significantly if the dielectric constant of the sorbed vapor, ϵ_v, differs greatly from that of the thiolate ligands. The variables

(26) Severin, E. J.; Lewis, N. S. *Anal. Chem.* **2000**, *72* (9), 2008−2015.
(27) Patel, S. V.; Jenkins, M. W.; Hughes, R. C.; Yelton, W. G.; Ricco, A. J. *Anal. Chem.* **2000**, *72* (7), 1532−1542.
(28) Swann, M. J.; Glidle, A.; Cui, L.; Barker, J. R.; Cooper, J. M. *Chem. Commun.* **1998**, *24*, 2753−2754.
(29) Hierlemann, A.; Zellers, E. T.; Ricco, A. J. *Anal. Chem.* **2001**, *73* (14), 3458−3466.
(30) Grate, J. W. *Chem. Rev.* **2000**, *100* (7), 2627−2647.
(31) Albert, K. J.; Walt, D. R.; Gill, D. S.; Pearce, T. C. *Anal. Chem.* **2001**, *73* (11), 2501−2508.
(32) Kummer, A. M.; Hierlemann, A.; Baltes, H. *Anal. Chem.* **2004**, *76* (9), 2470−2477.
(33) Patel, S. V.; Mlsna, T. E.; Fruhberger, B.; Klaassen, E.; Cemalovic, S.; Baselt, D. R. *Sens. Actuators, B* **2003**, *B96* (3), 541−553.
(34) Kim, B. H.; Prins, F. E.; Kern, D. P.; Raible, S.; Weimar, U. *Sens. Actuators B* **2001**, *B78* (1−3), 12−18.
(35) Senesac, L. R.; Dutta, P.; Datskos, P. G.; Sepaniak, M. J. *Anal. Chim. Acta* **2006**, *558*, 94−101.
(36) Terrill, R. H.; Postlethwaite, T. A.; Chen, C.; Poon, C.-D.; Terzis, A.; Chen, A.; Hutchison, J. E.; Clark, M. R.; Wignall, G.; Londono, J. D.; Superfine, R.; Falvo, M.; Johnson, C. S., Jr.; Samulski, E. T.; Murray, R. W. *J. Am. Chem. Soc.* **1995**, *117* (50), 12537−12548.
(37) Wuelfing, W. P.; Green, S. J.; Pietron, J. J.; Cliffel, D. E.; Murray, R. W. *J. Am. Chem. Soc.* **2000**, *122* (46), 11465−11472.
(38) Zamborini, F. P.; Smart, L. E.; Leopold, M. C.; Murray, R. W. *Anal. Chim. Acta* **2003**, *496* (1−2), 3−16.
(39) Hostetler, M. J.; Wingate, J. E.; Zhong, C.-J.; Harris, J. E.; Vachet, R. W.; Clark, M. R.; Londono, J. D.; Green, S. J.; Stokes, J. J.; Wignall, G. D.; Glish, G. L.; Porter, M. D.; Evans, N. D.; Murray, R. W. *Langmuir* **1998**, *14* (1), 17−30.
(40) Snow, A. W.; Wohltjen, H. *Chem. Mater.* **1998**, *10* (4), 947−949.
(41) Brust, M.; Bethell, D.; Schffrin, D. J.; Kiely, C. J. *Adv. Mater.* **1995**, *7* (9), 795−797.
(42) Neugebauer, C. A.; Webb, M. B. *J. Appl. Phys.* **1962**, *33*, 74−82.
(43) Neugebauer, C. A. *Thin Solid Films* **1970**, *6* (6), 443−447.
(44) Sheng, P.; Abeles, B. *Phys. Rev. Lett.* **1972**, *28* (1), 34−37.
(45) Abeles, B.; Sheng, P.; Coutts, M. D.; Arie, Y. *Adv. Phys.* **1975**, *24* (3), 407−461.
(46) Lu, C.-J.; Steinecker, W. H.; Tian, W.-C.; Oborny, M. C.; Nichols, J. M.; Agah, M.; Potkay, J. A.; Chan, H. K. L.; Driscoll, J.; Sacks, R. D.; Wise, K. D.; Pang, S. W.; Zellers, E. T. *Lab Chip* **2005**, *5* (10), 1123−1131.
(47) Zhong, Q.; Veeneman, R.; Steinecker, W.; Jia, C.; Batterman, S.; Zellers, E. T. *J. Environ. Monit.* **2007**, *9*, 440−448.
(48) Peak widths of <100 ms have been measured with a similar C8-MPN-coated CR sensor in a low-dead-volume detector cell downstream from a microfabricated column using a microfabricated pump for sample transport. Kim, H.; Steinecker, W. H.; Lambertus, G. R.; Astle, A. A.; Najafi, K.; Zellers, E. T.; Bernal, L. P.; Washabaugh, P. D.; Wise K. D. *Proceedings 10th International Conference on Miniaturized Systems for Chemistry and Life Sciences-μTAS '06*, Tokyo, Japan, November 5−9, 2006; pp 1037−1039.

r_c and δ in eq 2 account for the dependence of the intercore capacitance on the particle geometry.[45] Sorption of vapors with ϵ_v values significantly greater than ϵ_{th} could reduce E_a sufficiently to cause the film resistivity to decrease, which has been observed for some vapors.[6−13,21,22] For an increase in δ with a negligible change in ϵ_{th}, a small increase in E_a is expected, which marginally amplifies the resistance increase arising from the reduced tunneling probability (first term of eq 1).

Assuming that electronic conduction occurs by pathways that are randomly distributed throughout the MPN film, the CR resistance changes will be determined by the bulk film resistivity changes accompanying vapor sorption/desorption. Therefore, relative resistance changes are equivalent to relative resistivity changes (i.e., $\Delta R/R = \Delta\rho/\rho$), and CR vapor responses can be expressed as the fractional change in the resistance of the film arising from vapor sorption. From eq 1, we can then write

$$\frac{\Delta R}{R} + 1 = \frac{\rho_s}{\rho_o} = \frac{e^{\delta_s\beta} e^{E_{as}/kT}}{e^{\delta_o\beta} e^{E_{ao}/kT}} = e^{(\delta_s-\delta_o)\beta} e^{(E_{as}-E_{ao})/kT} = e^{\Delta\delta\beta+\Delta E_a/kT} \quad (3)$$

where the subscript s signifies a property evaluated when the film is swollen with vapor and the subscript o signifies a property evaluated when no vapor is present in the film. It is assumed that τ_o is independent of the vapor being present in the film.

Equation 3 relates measured sensor responses to the intercore spacing and the dielectric constant of the vapor-swollen ligand layer, but has limited practical utility because the variables are not readily accessible. It is useful at this point to introduce the partition coefficient, K, defined as the ratio of vapor concentrations in the sorbent phase, C_s, and in air, C_a, at equilibrium (i.e., $K = C_s/C_a$). K is a common metric of vapor uptake by sorptive microsensor interfaces and is often the primary determinant of relative responses among a set of vapors in a given microsensor interface layer.[26,30] Deriving a relationship between $\Delta R/R$ and K would be of considerable value, since it would provide a link between CR responses and the amount of vapor in the MPN film for a given vapor concentration. It would also permit the application of thermodynamic models of K, such as the linear solvation energy relationships that have been studied extensively in the context of polymer-coated acoustic-wave vapor sensors.[29,30]

Toward this end, we have derived the following expression relating relative resistance changes to K and C_a (the details and simplifying assumptions of this model derivation are provided in the Supporting Information):

$$\frac{\Delta R}{R} = e^{2\beta r_e\left(\left(1+\frac{C_aK}{d_v}\Psi_s\right)^{\frac{1}{3}}-1\right)} \times e^{\frac{e^2}{8\pi\varepsilon_o\varepsilon_{th}r_ckT}\left(\frac{1}{\left(1+\frac{C_aK}{d_v}\frac{d_{th}}{d_nw_{th}}\Psi_s\left(\frac{\varepsilon_v-\varepsilon_{th}}{\varepsilon_{th}}\right)\right)}\right)\left(1-\frac{r_c}{2r_e\left(1+\frac{C_aK}{d_v}\Psi_s\right)^{\frac{1}{3}}-r_c}\right)+\frac{r_c}{2r_e-r_c}-1\right)} - 1 \quad (4)$$

where d_v, d_n, and d_{th} are the densities of the analyte (vapor) in the liquid state, the MPN film (neglecting free volume), and the thiolate ligands, respectively, $r_e = \delta/2 + r_c$ is an "effective particle radius" (explained more completely in the Supporting Information), and w_{th} is the organic mass fraction of the MPN.

The variable Ψ_s is included in eq 4 to account for nonideal film swelling. For ideal cases, $\Psi_s = 1$. Nonideal film swelling may arise from significant cohesive forces between ligands and vapors, imperfect solvation of vapors by the ligands, or conformational constraints related to the ligands being tethered to the Au core. For MPNs, this would also address regions of low or imperfect inter-MPN ligand overlap and splay at the junctures of crystalline faces on the Au cores that may become occupied by vapor molecules without leading to a commensurate degree of film swelling.[39]

This model relates the response of an MPN-coated CR sensor explicitly to the relevant variables associated with the vapor, the nanoparticle, and their interaction. Vapor-specific variables include the d_v, ϵ_v, C_a, and K. MPN-specific variables include β, r_c, r_e, d_n, w_{th}, d_{th}, and ϵ_{th}. The intercore separation, δ, does not appear in these expressions, but is contained in the effective radius term, r_e. Mass uptake is represented by the quantity C_aK, where K reflects the interaction between the vapor and ligands. For a specific MPN, responses will vary only as a function of d_v, ϵ_v, C_a, K, and Ψ_s. In effect, Ψ_s serves as a weighting factor for C_aK/d_v, but will also account for any errors in the estimates of the MPN-specific variables, such as d_{th} or β.

Table 1. CR Device Dimensions and MPN Film Resistivity

device	electrode pairs	spacing (μm)	overlap (mm)	total area (mm^2)	ρ_o (kΩ·cm)[a]
A	20	15	1.4	1.7	337
B	18	1.0	0.046	0.0033	373
C	32	0.3	0.026	0.00099	−[b]

[a] Calculated from the slope of R vs h^{-1} (via eq 5) assuming $d_n = 3$ g/mL. [b] Estimates of ρ_o were not possible with this device due to film nonuniformities.

EXPERIMENTAL SECTION

Materials. Solvents were HPLC-grade or higher and were obtained from Fisher (Fairlawn, NJ) or Sigma-Aldrich (St. Louis, MO). Solvent purity was verified by GC. Free-radical scavengers in two of the chlorinated solvents (i.e., ethanol in chloroform and amylene oxides in 1,1,1-trichloroethane) were not removed prior to use. Alcohols were stored over molecular sieves. C8-MPNs were synthesized by the single-phase method of Rowe et al.[49] All data reported here were obtained from the same batch of C8-MPNs, which had an organic mass fraction of 16% and an average Au core diameter of 4.3 ± 0.9 nm.[49] C8-MPNs were stored as a dilute solution in toluene prior to use.

Sensor Preparation and Operation. CRs were constructed from three different interdigital electrode (IDE) designs (Table 1). Type A devices used sputter-deposited Au/Cr electrodes (400 nm of Au on 40 nm of Cr) patterned by a standard liftoff process on Si substrates pretreated with a thick thermally grown SiO_x layer for electrical isolation. Four type A devices, having IDE widths and spaces of 15 μm and a common ground, were made on a single chip.[15,46] Type B and C devices were constructed with sputtered Au/Cr electrodes (200 nm of Au on 20 nm of Cr)

(49) Rowe, M. P.; Plass, K. E.; Kim, K.; Kurdak, C.; Zellers, E. T.; Matzger, A. J. *Chem. Mater.* **2004**, *16* (18), 3513−3517.

patterned by electron-beam lithography with IDE widths and spaces of 1.0 (type B) and 0.3 μm (type C). One of each type of device was integrated on the same chip and connected to a common ground. The active areas of these devices are in the ratio of 1700:3.3:1.0 (A/B/C). Right-angled header pins were soldered onto the bonding pads of the type A devices to allow insertion into sockets on custom solder-down prototyping boards that carried reference resistors and connectors for power and signal transmission. One of these prototyping boards was placed in the exposure chamber, and another was used for spray coating. Type B and C devices were mounted on standard eight-pin carriers and connected with soldered wires. The carriers were then inserted into sockets on the prototyping boards.

A dc bias voltage (V_a) of 1.55 ± 0.01 V was applied to each device in series with a fixed resistor, R_1 (~1 MΩ), from a battery and the voltage drop across the CR sensor, V_c, was measured with a multiplexed, high-impedance, 22-bit digital volt meter (model 34970a with 34902a module, Agilent Technologies, Palo Alto, CA) and recorded at 10 Hz on a PC via a GP-IB connection using Agilent software. The sensor resistance, R_c, was then calculated from the relationship, $R_c = V_c R_1/(V_a - V_c)$. Values of V_c were typically in the range of 0.7−1.4 V and could be measured to ±0.5 μV, which corresponds to a resolution of 37.5 Ω (i.e., a $\Delta R/R$ of 3.75 ppm for a 10-MΩ baseline resistance). It was not necessary to fix the voltage drop of the CRs because linear I−V characteristics are observed over this voltage range at room temperature.

TSMRs 1.3 cm in diameter with rough gold electrodes (0.47 cm^2) and a resonant frequency of 10 MHz (Universal Sensors Inc., Metairie, LA) were driven by a phase-lock oscillator with capacitance compensation (model PLO-10i, Maxtek, Santa Fe Springs, CA). The frequency was measured at 1 Hz with a counter (53131A, Agilent Technologies) and recorded on a PC through a GP-IB interface. A stainless steel holder was fabricated in-house that clamped the TSMR crystal between a pair of Viton o-rings and isolated the backside from the test atmosphere. The holder screwed into the lid of the exposure chamber.

Prior to MPN deposition, all devices were washed with acetone, 2-propanol, and deionized water and then dried in a clean-air stream. CR substrates were then exposed to an oxygen plasma. TSMR substrates were not treated with plasma in order to avoid oxidation of the wires that provide electrical connections between the crystal and carrier. MPNs were deposited simultaneously on all CRs and on a TSMR placed in proximity by spray coating with an airbrush from dilute (~1−2% by mass) toluene solutions with pressure-regulated air as the propellant. CR resistances and the TSMR frequency were monitored over the course of the deposition. C8-MPN films ranged from 6.9 to 54 μg/cm^2 as determined from the TSMR frequency shift (1.6−12 kHz) via the Sauerbrey equation.[50] This corresponds to a nominal film thickness range of 23−180 nm assuming a density of 3 g/mL.[6,25,36,51] According to Grate et al.,[25] these thicknesses are well within the acoustically thin regime such that frequency shifts should accurately reflect mass changes. Coated-CR baseline resistances ranged from 3 to 75 MΩ depending on film thickness (see below).

Immediately following MPN deposition, sensors were placed in the 0.25-L stainless steel exposure chamber containing the prototyping board described above, electrical feed-throughs, and fluidic ports for gas inlet/outlet. Decreases in TSMR frequency (~1% relative to film mass) and CR resistances (up to 40%) were normally observed several hours postcoating, consistent with residual solvent loss. Typically, sensors were allowed to stand overnight in the exposure chamber under a clean-air flow prior to vapor exposures. The chamber temperature (23−25 °C) varied by less than 0.4 °C during a given series of measurements.

Vapor Exposures. Test atmospheres were generated by passing N_2 gas through fritted bubblers containing the liquid solvent and diluting with a metered air stream prepurified to remove trace organics and water vapor. A separate clean-air line was used to purge the exposure chamber after each exposure. Both clean and vapor-laden flow streams were maintained at 14 L/min (3-volume mixing time, 3.2 s) and toggled through a pair of Teflon three-way solenoid valves (648T033, NResearch, West Caldwell, NJ) either to the exposure chamber or to vent. Mass-flow controllers were used to adjust the vapor concentration, which was verified by periodically diverting aliquots to a GC-FID, precalibrated by liquid injection, via a six-port valve with a 0.25-mL sampling loop. At a given vapor concentration, duplicate or triplicate exposures were performed with a typical cycle consisting of a 5-min exposure followed by a 5-min purge with clean air. The concentration range over which calibrations were performed differed among the vapors because of the different vapor pressures and sensitivities observed, but typically spanned at least a ~10-fold range, never exceeded 20% of the saturation concentration, and started at the concentration yielding a signal of approximately five times the TSMR baseline noise level (starting concentrations ranged from 10 to 2000 ppm, and were typically <300 ppm). Plots of ΔR/R versus C_a for all vapors were, without exception, linear with near-zero intercepts. The CR signal-to-noise ratio was invariably greater that of the TSMR for the same vapor concentration (see below). Sensor and FID traces were imported to a chromatography software suite (Grams 32/AI 6.00, Galactic Industries, Salem, NH) for preprocessing, and the data were then exported to a spreadsheet program for final processing.

RESULTS AND DISCUSSION

General Features of MPN-Coated Sensors. Responses from CR sensors are rapid and reversible, with measured 1/e time constants for both response and recovery on the order of 1−5 s (full response/recovery times of 30−40 s) over the range of vapor concentrations and MPN layer thicknesses studied (23−180 nm), which approach the theoretical chamber mixing time (see Figure SI-1, Supporting Information, for representative response traces from both sensors). In the context of μGC detector applications,

(50) Ballantine, D. S., Jr.; White, R. M.; Martin, S. J.; Ricco, A. J.; Zellers, E. T.; Frye, G. C.; Wohltjen, H. *Acoustic Wave Sensors. Theory, Design, and Physico-Chemical Applications*; Academic Press: San Diego, CA, 1997.

(51) Densities in the range of 3−3.5 g/mL have been reported in refs 6 and 36 for C8-MPNs smaller than those used in this work. The value of 1.2 g/cm^3 reported in ref 14 on the basis of profilometer measurements of cast C8-MPN films appears to be in error. For the MPNs in this study, the estimated density is 4.3 g/mL if the ligand density is assumed to be that of liquid *n*-octanethiol (0.845 g/mL). For the purposes of estimating film thickness from TSMR-derived film masses, it is reasonable to assume a certain fractional free volume within the film. Grate et al. suggested a range of 0.26−0.32 in ref 25 that depends on assumed packing arrangements. Accordingly, we have adopted a value of 0.30 for thickness estimates. However, since the actual free volume could not be measured, it was neglected for purposes of estimating K values and modeling CR sensitivities. This will yield less conservative (i.e., higher) estimates of the partition coefficient for a given vapor. In the context of modeling sensor responses via eq 4, the influence of free volume is subsumed in the best-fit value for Ψ_s.

such rapid sorption/desorption kinetics facilitate sharp, symmetric peaks even for short detector cell residence times.[46−48]

C8-MPN-coated CR sensors prepared in our laboratory have maintained responses to toluene to within ±30% when measured periodically over a period of 4 years. However, fluctuations in toluene sensitivity of ±10% are typically observed over the span of a few days for both CR and TSMR sensors. Only a portion of this variation can be ascribed to temperature changes and calibration error. In addition, drifts in the CR baseline resistance of up to ±30% were observed without commensurate shifts in TSMR baseline frequencies, indicating that changes in the MPN film structure occur over time. While baselines were stable enough in the short term to obtain reproducible results during a given exposure series, we believe that small, random variations in interparticle ligand−ligand overlap are responsible for the baseline drift as well as a portion of the variation in vapor sensitivity. For experiments requiring more precise comparisons of responses, measurements were collected over short periods of time (hours) and toluene calibrations were used to confirm stability. Comparisons of data collected over longer periods of time relied on normalization to concurrently determined toluene and *n*-octane sensitivity values. Comparing across films, we have observed variations in baseline resistances as large as 60-fold (typically much smaller) for the same deposited mass, while relative resistance changes to a given toluene exposure varied by <40%. These observations are also consistent with variations in the degree of interparticle ligand overlap, which should affect the baseline resistance to a greater degree than vapor sensitivity.

Scaling Behavior. It was of interest to determine whether the model assumption that conduction pathways are randomly distributed throughout the MPN film would hold as the spacing of the IDE was reduced to submicrometer dimensions. The following equation describes the resistance of thin MPN layers measured with planar interdigital electrodes:[14,40]

$$R = \rho_o \frac{S_e}{(2n-1)L_e h} \tag{5}$$

where ρ_o is the bulk film resistivity, S_e is the interelectrode spacing, n is the number of electrode pairs (the quantity $2n - 1$ is the number of gaps), L_e is the electrode finger overlap, and h is the film thickness (assumed to be no greater than ~10× the electrode thickness). Plotting the CR baseline resistance, normalized by the geometric scaling factor $S_e/(2n - 1)L_e$, versus h^{-1} should yield a straight line with slope equal to ρ_o regardless of the IDE dimensions.

Figure 1 presents such a plot for type A, B, and C CR devices coated with successively thicker MPN layers in parallel with a TSMR. Values of h were estimated by dividing the film mass per unit area (from the TSMR frequency shift) by the nominal C8-MPN density of 3 g/mL. Each point for the type A design in Figure 1 is the average from the four devices (RSD < 7% for the four thickest films), while those for type B and C designs are individual measurements.

For the four thicker coatings in Figure 1, the type A and B devices give the expected linear relationship (r^2 > 0.98) with similar slopes and near-zero *y*-intercepts. Resistances higher than predicted by eq 5 are observed for the thinnest (i.e., 23-nm) films

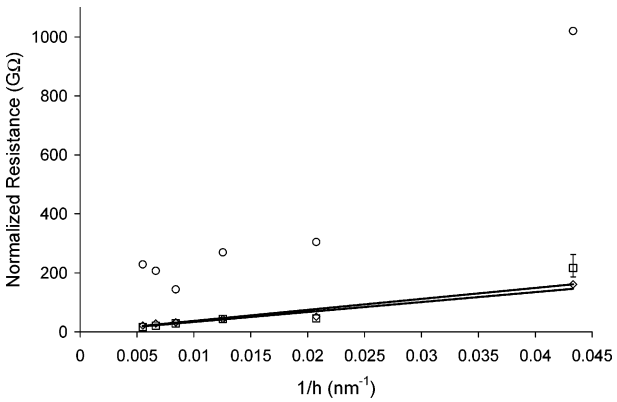

Figure 1. Plots of MPN-coated CR baseline resistance (dc), normalized by the IDE-geometry factor $S_e/[(2n - 1)L_e]$ (see eq 11), versus reciprocal MPN film thickness for type A (squares, S_e = 15 μm), type B (diamonds, S_e = 1 μm), and type C (circles, S_e = 0.3 μm). Lines were determined from regression using the four thickest MPN films on the type A and B devices. The slopes are equivalent to the MPN resistivity (see Table 1).

and can be attributed to film discontinuities and incomplete electrode coverage. This is most apparent on the type C device. Even the thicker film resistances measured with the type C device are inconsistent with eq 5: regression yields a finite *y*-intercept, an r^2 of only 0.91 and a slope that is ~ 6.5 times higher than those of the other two devices. SEM images (see Figure SI-2) reveal marked thickness variations over areas as small as 20−40 μm in deposited films. Given that the entire type C IDE array occupies an area of only 26 μm × 20 μm, its anomalous behavior can be explained by the resulting constraints on the number and distribution of conduction pathways. These nonuniformities are of little consequence on the larger type A and B devices.

Table 1 presents resistivities calculated from the slopes of the regression lines from Figure 1 for type A and B devices. The average ρ_o value of 340 kΩ·cm is higher than those reported by others for the same nominal materials.[14,20,36] Discrepancies may be due to differences in core diameters, ligand overlap, and synthetic method.[49,52] We note that in these other studies C8-MPNs were synthesized by use of the ionic phase-transfer catalyst tetraoctylammonium bromide, which can be difficult to remove from the final product[52] and has been shown to reduce baseline resistivities, presumably via contributions from ionic conduction or increases in ϵ_{th}. Assuming a resistivity of 340 kΩ·cm, the apparent coverage of the type C device ranges from 8 to 20%.

For the multilayer films obtained by spray coating, changes in thickness incurred upon vapor sorption are not expected to alter the number of conduction pathways, but rather only the conductivity of the existing network of pathways in the film. As long as the electric field strength does not vary significantly over the film cross section, the small increases in thickness accompanying vapor sorption will not affect the film resistance directly. Therefore, $\Delta R/R$ should be independent of electrode dimensions and film thickness.

Calibrations were performed with toluene for each of the coated devices at each thickness presented in Figure 1. Responses varied linearly with concentration and displayed near-zero *y*-

(52) Waters, C. A.; Mills, A. J.; Johnson, K. A.; Schiffrin, D. J. *Chem. Commun.* **2003**, 540−541.

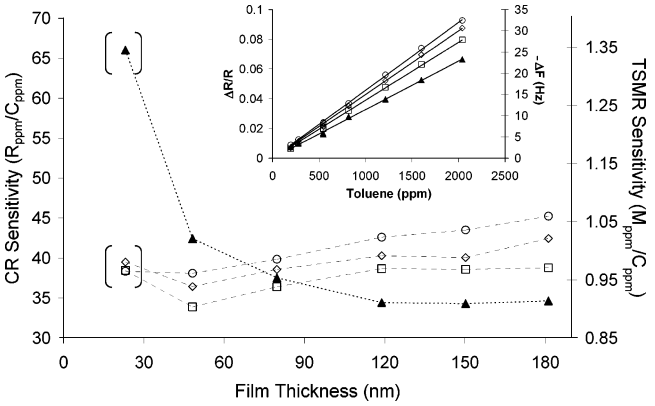

Figure 2. Toluene sensitivity as a function of C8-MPN thickness from 23 to 180 nm for type A (squares), type B (diamonds), and type C (circles) CR devices and for the TSMR (filled triangles). Fractional resistance changes are given in ppm relative to the baseline resistance (R_{ppm}). Fractional TSMR responses are given in ppm relative to the mass of film coating (M_{ppm}). Each point is the slope of the calibration curve determined by linear regression over a 10-fold range in toluene concentration (C_{ppm}). Points for the type A device are averages of four sensors, and the RSD at any thickness was <2%. The TSMR sensitivity value at 23 nm is interpolated from that at 48 nm and that due to adsorption on an uncoated device. The CR sensitivity values at 23 nm were estimated from this TSMR data point, due to a malfunction in the FID. The inset shows a representative set of calibration curves for 180-nm-thick films.

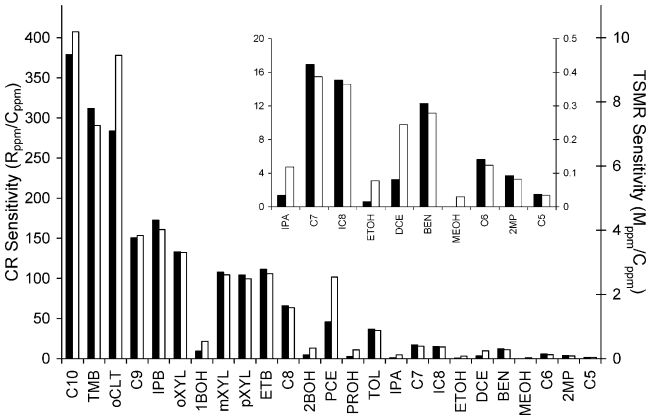

Figure 3. Sensitivities of C8-MPN-coated CR (type A, filled bars) and TSMR (open bars) sensors to each of 25 vapors determined from the slopes of the respective calibration curves. Analytes are arranged in order of increasing vapor pressure from left to right. Inset enlarges the right-most data for better visibility. Note the differences in the scales for the CR and TSMR.

intercepts for all sensors; linear regression with forced zero gave r^2 values of ≥0.997 in all cases (Figure 2, inset). Figure 2 summarizes the entire series of calibrations performed as a function of film thickness. For thinner films on the TSMR, there is a contribution from toluene adsorption on the roughened gold electrode, which becomes negligible above a thickness of 120 nm. The toluene sensitivities among the different CR devices varied by <7% (RSD) at any given film thickness. The linearity of the sorption isotherms coupled with the consistency of data among the devices of such widely differing areas (1700-fold range) and interface layer thicknesses (8-fold range) supports the assumption of bulk film vapor sorption and the applicability of the CR response model over this range of device dimensions. In spite of the apparent film discontinuities and consequently higher baseline resistances for the type C device (Figure 1), the sensitivity to toluene is not significantly different from those for the type A and B devices.

One of the important practical implications of these results relates to their use as detectors in a μGC. With most transducers (e.g., polymer-coated SAW resonators, capacitors, or cantilevers)[32,35,50,58] a reduction in the size of the device or the interface–film thickness (i.e., film volume) would be expected to change the sensitivity, as well as the signal-to-noise ratio (S/N). For an array, the sensor sensitivities define the response patterns used for vapor recognition and also directly impact the S/N and limit of detection (LOD). Provided that the detector cell volume can be reduced in proportion to the device area and that sorption kinetics are fast relative to cell residence times, the mass of vapor required to maintain sensitivities for MPN-coated CRs can be reduced in proportion to the area–thickness product (i.e., film volume), which in this case differs by 10^4-fold between type A and type C devices. This in turn translates into proportionally smaller injection masses required for an analysis, since noise levels were similar among these devices.[56] Where adsorbent preconcentrators are used to focus and thermally inject analyte vapors, this means that smaller preconcentrator bed masses can be used, producing sharper injections at reduced power dissipation; sampling times can also be reduced for higher temporal resolution of measurements.

To place these results in perspective, a recent study reported detection limits using an array of MPN-coated CR sensors (type A devices) corresponding to an injection mass of 0.47 ng of toluene (0.5 ppb in a 0.25-L preconcentrated sample).[46] The results obtained here suggest that the injected mass could be reduced to 0.047 pg (e.g., 0.5 ppb in 25 μL, assuming the same preconcentration factor) merely by reducing the size of the array.

Sensitivities and Analyte Physical Properties. Figure 3 summarizes sensitivity values for 25 vapors determined with TSMR and type A CR devices coated with 180-nm films of C8-MPN. The vapors are presented in order of increasing vapor pressure from left to right. Each bar is the slope of the calibration curve for each vapor (forced-zero regression r^2 values were >0.99 in all cases). As expected with sorptive interface layers,[59] sensitivity varies inversely with vapor pressure (see Table 2). In fact, for

(53) Howard, P. H., Meylan, W. M. Eds. *Handbook of physical properties of organic chemicals*; CRC-Lewis: Boca Raton, FL, 1997.
(54) Smith, B. D.; Srivastava, R. *Thermodynamic data for pure compounds*; Elsevier: New York, 1986.
(55) Weast, R. C., Ed. *CRC Handbook of Chemistry and Physics,* 76th ed.; CRC Press: Boca Raton, FL, 1995.

(56) A coated CR noise level of 1 ppm represents a typical resolution obtained after circuit optimization. Higher and lower values were observed. Observed noise levels were determined by the circuit components employed, since replacing the CR with a common resistor of identical resistance yielded no reduction in noise. This was true for type A, B, and C devices, indicating that the observed noise is independent of device size over the range examined here. MPN films have been shown to exhibit classical 1/*f* noise with a fundamental lower limit that is theoretically much lower than that reported here. With the proper implementation of analog circuitry for amplification and filtering, baseline noise could be reduced by 1 or 2 orders of magnitude (see ref 57).
(57) Kurdak, C.; Kim, J.; Kuo, A.; Lucido, J. J.; Farina, L. A.; Bai, X.; Rowe, M. P.; Matzger, A. J. *Appl. Phys. Lett.* **2005**, *86* (7), 073506.
(58) Grate, J. W.; Klusty, M. *Anal. Chem.* **1991**, *63*, 1719–1727.

Table 2. Vapor Properties, Sensor Performance Metrics, and Errors in Modeled CR Sensitivities[a]

vapor (abbreviation)	p_v (Torr)	d_v (g/mL)	ϵ_v	K[b]	CR[c] sensitivity	CR LOD[d] (ppm)	TSMR LOD[e] (ppm)	error[f] (%)
n-butane (C_4)	1820	0.572						
n-pentane (C_5)	510	0.619	1.84	51	1.5	2.0	4300	−0.2
2-methylpentane (2MP)	210	0.649	1.89	100	3.7	0.81	1800	−10
chloroform (CHL)	197	1.498	4.71					
n-hexane (C_6)	150	0.657	1.88	150	5.6	0.53	1200	−11
methanol (MEOH)	130	0.784	32.6	97	−0.020	150	5100	149
1,1,1-trichloroethane (TCA)	124	1.338	7.08					
benzene (BEN)	95	0.874	2.27	380	12	0.24	540	−7
1,2-dichloroethane (DCE)	79	1.246	10.1	260	3.3	0.92	610	15
ethanol (ETOH)	59	0.782	24.9	180	0.60	4.9	1900	−8
2,2,4-trimethylpentane (IC_8)	49	0.686	1.94	340	15	0.20	410	−7
n-heptane (C_7)	46	0.679	1.91	410	17	0.18	390	−11
2-propanol (IPA)	45	0.781	19.3	210	1.4	2.2	1300	18
toluene (TOL)	28	0.862	2.37	1000	37	0.082	170	−1
1-propanol (PROH)	21	0.796	20.5	480	2.7	1.1	540	24
perchloroethylene (PCE)	19	1.614	2.27	1600	46	0.065	59	−10
2-butanol (2BOH)	18	0.796	15.9	460	4.7	0.64	460	20
n-octane (C_8)	14	0.698	1.94	1500	66	0.046	95	−9
ethylbenzene (ETB)	9.6	0.862	2.43	2600	110	0.027	57	−2
p-xylene (pXYL)	8.8	0.857	2.27	2500	100	0.029	60	−0.5
m-xylene (mXYL)	8.3	0.860	2.35	2600	110	0.028	57	0.6
1-butanol (1BOH)	6.7	0.802	17.3	760	9.4	0.32	280	−10
o-xylene (oXYL)	6.6	0.876	2.55	3300	130	0.023	45	0.7
isopropylbenzene (IPB)	4.5	0.858	2.37	3500	170	0.017	37	−3
n-nonane (C_9)	4.5	0.714	1.96	3100	150	0.020	39	−5
o-chlorotoluene (oCLT)	3.4	1.083	4.63	7900	280	0.011	16	1
1,3,5-trimethylbenzene (TMB)	2.5	0.860	2.27	6400	310	0.010	21	−3
n-decane (C_{10})	1.4	0.730	1.98	7500	380	0.0079	15	−3

[a] Physical properties obtained from refs 53−55. [b] Vapor−MPN partition coefficient calculated by assuming an average C8-MPN density of 4.3 g/mL. [c] Units, R_{ppm}/C_{ppm} (see text). [d] Calculated using 3σ/sensitivity, assuming a baseline noise (σ) of 1 ppm. [e] Calculated by assuming a baseline noise of 50 ppb. [f] Error in predicted CR sensitivity using eq 4 with the K, d_v, and ϵ_v values in this table, assuming $\Psi_s = 0.319$ for aromatic vapors and $\Psi_s = 0.233$ for all other vapors (see text). Sensitivity data are not reported for CHL and TCA because of impurities (see text) or for butane because the concentrations necessary to generate quantifiable CR and TSMR responses yielded FID responses that exceeded the electrometer maximum output.

both sensors, plots of sensitivity (normalized by molecular weight) versus $1/p_v$ are approximately linear ($r^2 \sim 0.90$, data not shown) for all of the nonpolar compounds (alcohols are described by a separate linear plot for each sensor, consistent with their higher sorption enthalpies).[59] Observed deviations from linearity for the CR are consistent with dielectric effects and swelling efficiency differences among the vapors, as discussed below. The latter also appears to be important for the TSMR. This topic will be discussed in a subsequent article. The strong correlation between the responses of the two types of sensors arises from their predominant dependence on K.

Several features of this data set are noteworthy. First, the fractional resistance changes of the CR are much larger than the fractional mass changes of the TSMR (note the scale difference for the CR and TSMR sensitivities in Figure 3). In fact, these CR/TSMR sensitivity ratios are approximately 30−40 times higher than ratios reported by Cooper et al. using poly(ethylene oxide) CLIP-coated CRs.[28] They are comparable to, though generally larger than, those reported recently by Yang et al. for C8-coated MPNs.[20] This indicates that the fractional resistance change achieved with MPN-coated CR sensors per mass of sorbed analyte is substantially higher than that for typical CLIP-coated CR sensors. Table 2 presents sensitivities and LODs for the vapors on both sensors, using rms noise levels of 1 ppm for the CR and 50 ppb for the TSMR.[56] CR sensitivities are similar (i.e., within a factor of 2) to those reported in ref 15 for five of the six vapors common to both studies (the exception is ethanol, for which our sensitivity is significantly lower). The toluene sensitivity reported here is also within a factor of 2 of that reported by Pang et al.[22] The significantly lower LODs obtainable with the CR sensor relative to the TSMR are consistent with previous reports,[6,14,20] and support the hypothesis[25] that transduction in MPN-coated CRs is more efficient than in similarly coated TSMRs.

A second notable feature of Figure 3 is that the TSMR/CR sensitivity ratios are significantly greater for the alcohols and the higher density nonpolar vapors than for the lower density nonpolar vapors: the ratios for oCLT, DCE, and PCE (d_v = 1.1, 1.3, and 1.6 g/cm^3, respectively) are all greater than those for the lower density vapors and also increase with density. For the alcohols, with very similar densities, the high TSMR/CR ratios and the trend in those ratios along the homologous series are attributable to their ϵ_v values as discussed below.

Vapor Density and Dielectric Constant. Figure 4 plots the sensitivity ratios derived from the data in Figure 3 versus the liquid density of each analyte. For the relatively nonpolar vapors with low and similar dielectric constants, there is indeed a strong linear correlation (open circles in Figure 4, $r^2 = 0.87$). Thus, densitometry is possible for vapors with dielectric constants falling within a narrow range using this two-sensor "hybrid array".[26,28] From the

(59) (a) Hierlemann, A.; Ricco, A. J.; Bodenhöfer, K; Dominik, A.; Göpel, W. *Anal. Chem.* **2000**, *72*, 3696−3708. (b) Patrash, S. J.; Zellers, E. T. *Anal. Chem.* **1993**, *65*, 2055−2066.

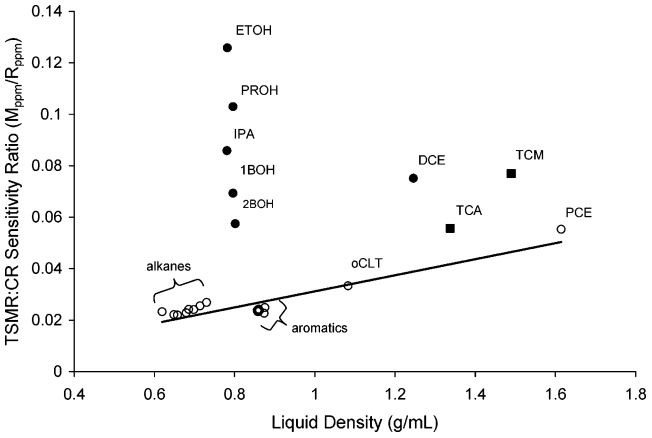

Figure 4. TSMR:CR sensitivity ratio vs liquid analyte density. The regression line shown was plotted using only those data points represented as open circles (see text for explanation).

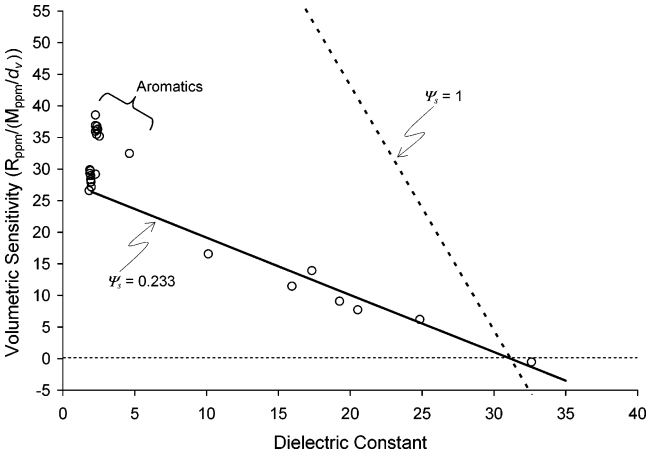

Figure 5. CR:TSMR sensitivity ratio, normalized by the vapor density, vs vapor dielectric constant. The ordinate variable represents the sensitivity of the CR to changes in sorbed vapor volume. Dashed line is the modeled prediction assuming ideal swelling, and the solid line is the model prediction assuming a swelling efficiency of 0.233 (based on pentane).

slope of the line in Figure 4, the response ratio changes at a rate of 0.031 per g/mL and the minimum resolvable density difference is ~0.1 g/mL, indicating that discrimination could be enhanced by the difference in the volume occupied by a given mass of absorbed vapor.[60]

The response ratios for the alcohols fall on a nearly vertical line in Figure 4, due to the similarities in their densities, and track their ϵ_v values. Methanol was omitted from Figure 4 because its CR responses, while linearly related to concentration, are all negative (note: responses to water vapor were unambiguously negative, but could not be quantified due to the very low signal-to-noise ratios). The ordinate values in Figure 4 are independent of vapor concentration and vapor−MPN partition coefficients. Thus, the trend in the alcohol data arises entirely from the dependence of the CR response on ϵ_v: the greater the difference in ϵ_v and ϵ_{th}, the lower the response per unit mass of vapor in the film.

The two vapors represented by the filled squares in Figure 4 are chloroform and 1,1,1-trichlorethane (d_v = 1.49 and 1.34 g/cm^3, respectively), which have dielectric constants of 4.71 and 7.08, respectively, and so would be expected to lie above the line drawn for the low-dielectric-constant vapors. However, both should fall closer to the line and the chloroform should be lower than the 1,1,1-trichloroethane. These apparent anomalies can be explained by the presence of stabilizing agents (see Experimental Section). The positions on the plot for these 'mixtures' reflect the influence that even a small fraction of a high-ϵ_v vapor has on the CR responses. The one remaining non-alcohol vapor that falls above the line is 1,2-dichloroethane, which has a relatively high ϵ_v value of 10.1 and is at an appropriate location on the plot.

Similar correlations of TSMR:CR ratios with vapor density have been reported for the CLIP-coated CR sensors referred to above.[26,28] However, in those reports, the alcohols and other polar, high-ϵ_v vapors did not show any difference in correlation from those of the nonpolar vapors. This would seem to be due to the use of polymers in those studies that are polar and presumably have dielectric constants higher than that of C8-MPN. As a result, the influence of ϵ_v on response ratios is reduced. Other researchers have collected TSMR and CR responses for various MPNs but did not focus on these correlations.[12,18,20,23,24]

Figure 5 shows a plot of a term representing the "volumetric sensitivity" of the CR sensor versus ϵ_v for all 25 vapors. Values of volumetric sensitivity were obtained by taking the inverse of the response ratios used in Figure 4 and then dividing by d_v. In this way, the effect of analyte density on the CR response is absorbed into the ordinate variable. The trend reflects the countervailing effect exerted by the vapor dielectric constant, via a decrease in E_a (vida supra), on the CR sensitivity to swelling-induced volume changes in the film. The aliphatic and aromatic hydrocarbons are clustered to the left side of this plot because of the similarity in their ϵ_v values. Regressing ϵ_v onto volumetric sensitivity for the high-ϵ_v vapors yields a straight line (r^2 = 0.90, not shown) and an estimated resolution of ~2ϵ_v units. Thus, as with vapor density, analyte discrimination should also be enhanced by this contribution to the CR response. According to the model, the sensitivity to ϵ_v depends explicitly on the starting value of ϵ_{th}, decreasing as ϵ_{th} increases (see Figure SI-4).

Response Model Validation. Equation 4 predicts CR relative responses to vary in a nonlinear manner with the partition coefficient, intercore separation, vapor density, dielectric constant, and vapor concentration (see Figure SI-3 for a complete response isotherm predicted for *n*-octane). However, if the concentration range is constrained to less than ~20% of saturation, predicted response curves are linear, as observed experimentally. For the modeled data presented below, responses were predicted using eq SI-6 for a series of uptake concentrations (i.e., m_v/m_n) ranging from 1 to 20 ppm to ensure that responses were in the linear range. These film concentrations were converted to the corresponding air concentrations using the appropriate K values. Regression of the predicted relative responses onto the air concentrations yielded the modeled CR sensitivity. Alternatively, the CR sensitivity could be determined by evaluating eq 4 for an assumed (low) C_a value and then dividing the predicted response by that value of C_a.

The trends shown in Figures 4 and 5 are qualitatively consistent with the response model. To assess the performance of the model quantitatively requires that the MPN-specific variables β, ϵ_{th}, r_c, d_n, w_{th}, d_{th}, and δ be specified. We have chosen

(60) Grate, J. W.; Wise, B. M. *Anal. Chem.* **2001**, *73*, 2239−2244.

a value of $\beta = 1.2$ Å^{-1}, which appears to be the most accurate of those reported for *n*-alkanethiolate MPNs (range, 0.8−1.2 Å^{-1}).[36−38] A value of $\epsilon_{th} = 2.83$, close to the value of 2.6 reported by Porter et al. for *n*-alkanethiolate SAMs on planar Au surfaces,[61] was found to give best agreement with experimental data. From ligand lengths reported by Porter et al.[61] and assuming full intercalation of ligands on adjacent MPNs (such that $\delta = 1.2 \times$ ligand length),[36] we calculated a δ of 1.76 nm for the unswollen C8-MPNs. Measured values of $r_c = 4.3$ nm and $w_{th} = 0.16$ were used and a $d_n = 4.3$ g/mL was calculated from published densities of Au and *n*-octanethiol (i.e., 19.3 and 0.845 g/mL, respectively). Inclusion of 30% free volume yields the d_n value of 3 g/mL used for estimating film thicknesses above. Since free volume is not included explicitly in the model and may vary with deposition conditions and core size, it was deemed more appropriate to use the "ideal" value of 4.3 g/mL[51] for modeling, thereby lumping any free-volume effects in with Ψ_s.

Using the densities and dielectric constants of the vapors and the values of the MPN-specific variables discussed above with an ideal $\Psi_s = 1$, eq 4 (or eq SI-6) accurately predicts the trend observed in the data in Figure 5 but overestimates the volumetric sensitivity by a factor of 3−4 (dashed line in Figure 5). Since only a fraction of the sorbed vapor volume will contribute to a commensurate increase in intercore distance, it is reasonable to expect that Ψ_s will, in fact, be less than unity. Adjusting Ψ_s should provide a way to more closely reconcile the modeled data with those determined experimentally.

In order to assign a Ψ_s value, a reference vapor is needed. We chose *n*-pentane for this purpose because it should be easily accommodated within the ligand matrix even with highly intercalated ligands. For pentane, the value of Ψ_s required to fit the modeled volumetric sensitivity to that observed experimentally is 0.233. Using this value in the model over the relevant range of ϵ_v values yields the solid line shown in Figure 5. Agreement with the data is quite good for the aliphatics, chlorinated aliphatics, and alcohols. Agreement is not as good for the aromatic vapors. If toluene is used as the reference vapor instead of pentane, then a swelling efficiency of 0.319 is obtained. This improves the fit for the aromatic vapors but reduces it for most of the other vapors (i.e., the slope and *y*-intercept of the line both increase). Note that regardless of swelling efficiency, the *x*-axis intercept of the line derived from the model in Figure 5 remains constant, as it is determined by ϵ_{th}. The extent to which ϵ_{th} and Ψ_s affect the dependence of the volumetric sensitivity on ϵ_v is illustrated more generally in Figures SI-4 and SI-5.

Thus, a single swelling efficiency value cannot reconcile all of the data with high fidelity. Figure 6 shows a plot of CR sensitivity per mole of vapor in the film (based on mass uptake measured by TSMR, normalized by film mass) versus the molar volume of each of the alkanes and aromatic hydrocarbons. Sensitivity increases linearly from C_4 to C_8, but the curve becomes slightly concave downward from C_8 to C_{10}. The molar sensitivities for the aromatic vapors are consistently higher than those for the alkanes of similar molar volume, in spite of their higher ϵ_v values. This indicates that the alkane molecules are sorbed more efficiently into the MPN ligand matrix than the aromatic molecules. Put another way, the aromatics are more effective in swelling the MPN film. Apparently, as the alkane chain length increases it is less easily accommodated within the ligand matrix and the swelling efficiency is reduced. For the series of aromatics examined here, the swelling efficiency is nearly invariant.

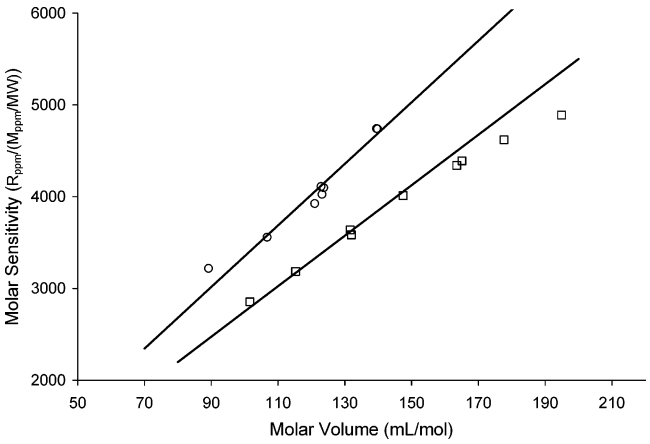

Figure 6. CR sensitivity per mole of sorbed vapor vs the (liquid-phase) molar volume for a series of alkanes (squares) and aromatic compounds (circles). Alkanes (left to right): *n*-butane, *n*-pentane, *n*-hexane, 2-methylpentane, *n*-heptane, *n*-octane, 2,2,4-trimethylpentane, *n*-nonane, *n*-decane; Aromatics (left to right): benzene, toluene, *o*-xylene, ethylbenzene, *m*-xylene, *p*-xylene, 1,3,5-trimethylbenzene, and isopropylbenzene. Lines represent least-squares regression fits derived from all of the aromatic vapors (upper) and from C_4 to C_8 alkanes (lower), with *y*-intercepts forced to zero.

As a final test of the model, the CR sensitivities for all of the vapors were estimated using the appropriate values of K, ϵ_v, d_v, and a Ψ_s of either 0.233 or 0.319, depending on whether the vapor was aromatic or not. Errors in the estimates are listed in the last column of Table 2. Excluding methanol, which gives a very low response and therefore an inflated relative error, the largest absolute error is 24% and most errors are <10%. Estimates for high-ϵ_v vapors give fractional errors that are also inflated by the exceptionally low CR sensitivities (e.g., methanol). Thus, reasonably accurate predictions of responses are possible. If just a single swelling efficiency value is used (i.e., $\Psi_s = 0.28$), the maximum error is still <42% (excluding methanol, 200%) and is typically <20%. The plot of experimental versus modeled sensitivities gives a slope of 1.0 and $r^2 = 0.97$.

Figure SI-6 summarizes how the predicted CR sensitivity varies over typical ranges of the key vapor-specific variables, assuming a single Ψ_s value of 0.28. To allow presentation in three dimensions, the ratio of the partition coefficient and density has been used as a composite independent variable, representing the "volumetric partition coefficient". Agreement between model and experiment is shown to be reasonably good despite the use of a single Ψ_s value. This allows, for the first time, a direct comparison of sorption and dielectric effects on MPN-coated CR sensor responses.

CONCLUSIONS

The model derived here parametrizes the contributions of the relevant variables associated with the analyte vapor, the MPN interface film, and the vapor−MPN interactions to the response of an MPN-coated CR sensor. It thereby provides a framework within which the influence of key variables on those responses

(61) Porter, M. D.; Bright, T. B.; Allara, D. L.; Chidsey, C. E. D. *J. Am. Chem. Soc.* **1987**, *109* (12), 3559−3568.

can be examined and understood. For this initial study, we have explored the implementation of the model for a gold−octanethiolate MPN interface layer. Its application to MPNs with different thiolate−ligand functionalities is currently being explored. Provided that values of the required MPN-specific variables (i.e., β, ϵ_{th}, d_n, d_{th}) are available, the model accurately predicts CR responses to a wide range of vapors with just a single adjustable parameter (i.e., the swelling efficiency).

The assumption that tunneling currents (and vapor-induced modulations thereof) are generated through the entire MPN film volume was shown to hold for film volumes spanning a range of 10^4. Since size reductions lead to faster sensor response times without loss of sensitivity, the remarkably low LODs observed here with relatively large (type A) devices, which are projected to be in the low-ppb range for the less-volatile analytes examined here, should be preserved in sensors several orders of magnitude smaller. In the context of microanalytical system design, smaller sensors translate to proportionally smaller required sample masses, and any upstream preconcentrator or separation module employed can be scaled down accordingly. This facilitates sharper injections, which permit faster elution times at higher resolution, shorter sampling cycles, and reduced column/preconcentrator heater power dissipation.

The ratio of responses of TSMR and CR sensors varies in a predictable manner with the vapor density and dielectric constants using the same MPN material as the interface layers. Since MPNs with different ligand functionalities should exhibit different sensitivities to the vapor dielectric constant (and possibly vapor density), it should be possible with a simple array to determine the vapor density and dielectric constant. This information, when added to the differential partitioning among MPN films, would increase the capability for vapor recognition. Should the systematic swelling efficiency differences observed here between aromatic and aliphatic vapors prove to persist among other MPN ligand types, this provides yet another possible discriminating variable for vapor recognition. The simpler approach of an all-CR array comprising CR sensors with different MPN interface layers affords access to the same vapor descriptors but would rely on relative differences in their values for discrimination. Still, the "design space" is quite wide.

ACKNOWLEDGMENT

The authors express their heartfelt appreciation to Mr. Don E. George for guidance in analog circuitry, Mr. Albert G. Wilson for training in precision machining and component design, Professor Chia-Jung Lu for valuable insights on fluidics and electronics, and Prof. Çagliyan Kurdak for assistance in fabricating type B and C devices and informative discussions on electron transport through nanoparticle films. This work was supported through the Michigan Center for Wireless Integrated Microsystems by the Engineering Research Centers Program of the National Science Foundation under Award ERC-9986866. Additional support was provided by Grant R01-OH03692-06 from the National Institute for Occupational Safety and Health of the Centers for Disease Control and Prevention.

SUPPORTING INFORMATION AVAILABLE

Derivation of the response model for an MPN-coated CR vapor sensor in addition to a series of figures illustrating various aspects of the MPN-coated CR and TSMR sensors and their predicted behavior. This material is available free of charge via the Internet at http://pubs.acs.org.

Received for review January 11, 2007. Accepted April 18, 2007.

AC070068Y